

Native point defects and dangling bonds in α -Al₂O₃

Minseok Choi, Anderson Janotti, and Chris G. Van de Walle

Citation: *J. Appl. Phys.* **113**, 044501 (2013); doi: 10.1063/1.4784114

View online: <http://dx.doi.org/10.1063/1.4784114>

View Table of Contents: <http://jap.aip.org/resource/1/JAPIAU/v113/i4>

Published by the [American Institute of Physics](#).

Related Articles

Inversion domain boundaries on tin (Sn)-doped ZnO nanobelts: Aberration-corrected scanning transmission electron microscopy study

Appl. Phys. Lett. **102**, 033103 (2013)

Interstitial Ti for intermediate band formation in Ti-supersaturated silicon

J. Appl. Phys. **112**, 113514 (2012)

Room-temperature method for minimizing light-induced degradation in crystalline silicon

Appl. Phys. Lett. **101**, 232108 (2012)

Unexpected positive role of oxygen vacancies in Na-doped ZnO

J. Appl. Phys. **112**, 113510 (2012)

Investigating thermal donors in n-type Cz silicon with carrier density imaging

AIP Advances **2**, 032169 (2012)

Additional information on *J. Appl. Phys.*

Journal Homepage: <http://jap.aip.org/>

Journal Information: http://jap.aip.org/about/about_the_journal

Top downloads: http://jap.aip.org/features/most_downloaded

Information for Authors: <http://jap.aip.org/authors>

ADVERTISEMENT



AIP Advances

Now Indexed in Thomson Reuters Databases

Explore AIP's open access journal:

- Rapid publication
- Article-level metrics
- Post-publication rating and commenting

Native point defects and dangling bonds in α -Al₂O₃

Minseok Choi,^{a)} Anderson Janotti, and Chris G. Van de Walle

Materials Department, University of California, Santa Barbara, California 93106-5050, USA

(Received 6 November 2012; accepted 2 January 2013; published online 22 January 2013)

We performed hybrid functional calculations of native point defects and dangling bonds (DBs) in α -Al₂O₃ to aid in the identification of charge-trap and fixed-charge centers in Al₂O₃/III-V metal-oxide-semiconductor structures. We find that Al vacancies (V_{Al}) are deep acceptors with transition levels less than 2.6 eV above the valence band, whereas Al interstitials (Al_i) are deep donors with transition levels within ~ 2 eV of the conduction band. Oxygen vacancies (V_O) introduce donor levels near midgap and an acceptor level at ~ 1 eV below the conduction band, while oxygen interstitials (O_i) are deep acceptors, with a transition level near the mid gap. Taking into account the band offset between α -Al₂O₃ and III-V semiconductors, our results indicate that V_O and Al DBs act as charge traps (possibly causing carrier leakage), while V_{Al} , Al_i , O_i , and O DBs act as fixed-charge centers in α -Al₂O₃/III-V metal-oxide-semiconductor structures. © 2013 American Institute of Physics. [<http://dx.doi.org/10.1063/1.4784114>]

I. INTRODUCTION

There is great interest in developing metal-oxide-semiconductor (MOS) devices based on III-V semiconductors, adding flexibility to the device design and enabling novel functionalities in III-V semiconductor-based electronics.¹ A large part of this effort involves identifying and optimizing suitable oxide dielectrics that can be built into oxide/III-V MOS structures, minimizing the concentration of charge-trap and fixed-charge centers, and lessening current leakage. Promising results have been achieved with Al₂O₃ as a gate dielectric in III-V-based MOS devices, with interfacial densities of states of $\sim 10^{12}$ /cm² eV at the Al₂O₃/III-V interface.^{2–7} The origin of the observed charge traps and fixed charges at the Al₂O₃/III-V interfaces, particularly in the GaN-based MOS structures, remains unknown, being most likely due to point defects in the oxide, located at or near the interface. Further improvements in device performance rely on understanding the structural and electronic characteristics of point defects in the oxide and their impact on the electronic properties of the oxide/III-V interface.

Here, we perform first-principles calculations for native point defects and dangling bonds (DBs) in Al₂O₃, with the intent of identifying possible defects that can give rise to charge traps and fixed-charge centers in Al₂O₃/III-V MOS structures. The information generated here will also be useful in the context of many other applications of alumina. α -Al₂O₃ with the corundum structure is used in high-temperature structural ceramics, optical devices, and in thermoluminescence for dosimetry.

First-principles calculations for native point defects in α -Al₂O₃ have already been reported.^{8–10} However, most of these calculations were carried out using the local density approximation (LDA) or the generalized gradient approximation (GGA) within density functional theory (DFT), thus, resulting in a large band-gap error, and making it very difficult to predict, with sufficient precision, the position of the

defect levels with respect to the band edges. For example, Matsunaga *et al.*⁸ find that oxygen vacancies (V_O) introduce donor transition levels at 5.0 eV above the valence-band maximum (VBM), while Hine *et al.*¹⁰ find the same transition levels at 3.5 eV above the VBM. The disagreement in the position of the V_O -related levels is likely associated with the difference in the procedure adopted to overcome the band-gap problem: Matsunaga *et al.*⁸ rigidly shift the occupied states in the gap with the conduction band in order to match the experimental band gap; Hine *et al.*,¹⁰ on the other hand, project the defect-related Kohn-Sham gap states onto the valence- and conduction-band states. This projection is then used to correct the position of the occupied gap states, and the formation energy is corrected according to the occupation of these states and their fraction of conduction-band character. Both approaches unjustifiably assume that the band-gap error only affects the conduction-band states.

Here, we avoid these difficulties by using a method that overcomes the band-gap problem and allows for calculations of total energies and lattice relaxations within the same framework. Hybrid functionals, which mix GGA with a non-local Hartree-Fock exchange potential, allow a more accurate description of band structures, and have provided more reliable descriptions of the defect-level positions in wide-band-gap semiconductors and oxides.^{11–17} Details of the methodology are provided in Sec. II.

We have carried out hybrid functional calculations for point defects on both Al and O sublattices in α -Al₂O₃, as reported in Sec. III A. The impact of these defects on the electronic properties of Al₂O₃/III-V interfaces is analyzed by inspecting defect formation energies and positions of transition levels, taking into account the band alignment between Al₂O₃ and III-V semiconductors, as discussed in Sec. III C. Calculations for point defects in κ -Al₂O₃, another phase of Al₂O₃, were previously reported;^{18,19} a comparison with those results will be discussed.

Al₂O₃ as a dielectric in gate stacks is most often deposited using the atomic layer deposition (ALD) technique, resulting in amorphous material. The local environment in

^{a)}Electronic address: minseok@engineering.ucsb.edu.

such amorphous structures is similar to that in the crystalline material, and hence our results for point defects in the crystalline phase are relevant. Amorphous material may also contain DB defects, however. In addition, due to the lattice mismatch and chemical mismatch between Al_2O_3 and III-V semiconductors, DBs may also occur at the interface between the two materials. Results for DBs on the oxygen as well as aluminum sites are discussed in Sec. III B.

II. METHODOLOGY

The calculations were performed using the screened hybrid functional of Heyd-Scuseria-Ernzerhof (HSE),^{20,21} implemented with the projector augmented-wave method²² in the Vienna *Ab initio* Simulation Package (VASP) code.²³ The mixing parameter in the HSE was set to 32%, which yields a 9.2 eV band gap for $\alpha\text{-Al}_2\text{O}_3$, similar to the reported experimental values of 8.8 eV (Ref. 24) and 9.4 eV (Ref. 25). The calculated lattice parameters of $a = 4.74 \text{ \AA}$ and $c = 12.94 \text{ \AA}$ are very close to the experimental values of $a = 4.76 \text{ \AA}$ and $c = 12.99 \text{ \AA}$.²⁶ In the $\alpha\text{-Al}_2\text{O}_3$, each Al is bonded to six O and each O is surrounded by four Al. The Al–O bond lengths are computed to be 1.85 \AA for three shorter and 1.96 \AA for three longer bonds, which are in a good agreement with the experimental values of 1.86 and 1.97 \AA .²⁶

Defect calculations were performed using periodic boundary conditions with a supercell containing 120 atoms, and the integrations over the Brillouin zone were performed using a $2 \times 2 \times 1$ k -point grid. The electronic wave functions were expanded in a plane-wave basis set with an energy cutoff of 400 eV. The effects of spin polarization were included. The atomic coordinates were relaxed until the Hellmann-Feynman forces acting on each atom were reduced to less than 0.05 eV/ \AA .

The formation energy of a defect D in charge state q is given by^{27,28}

$$E^f(D^q) = E_{\text{tot}}(D^q) - E_{\text{tot}}(\text{Al}_2\text{O}_3) - \sum_i n_i (\mu_i^0 + \mu_i) + q\epsilon_F + \Delta^q, \quad (1)$$

where $E_{\text{tot}}(D^q)$ is the total energy of a supercell containing the defect D in charge state q , and $E_{\text{tot}}(\text{Al}_2\text{O}_3)$ is the total energy of Al_2O_3 in the same supercell. n_i is the number of atoms of type i added to ($n_i > 0$) and/or removed from ($n_i < 0$) the perfect crystal to form the defect, and μ_i ($i = \text{Al}$ and O) are the atomic chemical potentials. ϵ_F is the Fermi level referenced to the valence band maximum (VBM), and Δ^q is the correction term to align the electrostatic potentials of the bulk and defect supercells and to account for finite-cell size effects on the total energies of charged defects.^{29,30} μ_{Al} is referenced to the total energy per atom of Al metal [$\mu_{\text{Al}}^0 = E_{\text{tot}}(\text{Al})$], and μ_{O} is referenced to the total energy per atom of an isolated O_2 molecule [$\mu_{\text{O}}^0 = (1/2)E_{\text{tot}}(\text{O}_2)$]. Our HSE calculations produce very good results for the binding energy and equilibrium bond length of the O_2 molecule. The calculated binding energy and bond length are 4.98 eV and 1.21 \AA , in good agreement with the experimental values (5.12 eV, 1.21 \AA)³¹ as well as with recent hybrid functional calculations using a linear combination of atomic orbitals (LCAO) basis set (5.30 eV, 1.20 \AA).³²

The chemical potentials μ_{Al} and μ_{O} are variables that must satisfy the stability condition of Al_2O_3 , $2\mu_{\text{Al}} + 3\mu_{\text{O}} = \Delta H_f(\text{Al}_2\text{O}_3)$ with $\mu_{\text{Al}} \leq 0$ and $\mu_{\text{O}} \leq 0$, and can be set to correspond to specific growth or annealing conditions. For instance, in the extreme O-rich (Al-poor) condition we have $\mu_{\text{O}} = 0$ and $\mu_{\text{Al}} = (1/2)\Delta H_f(\text{Al}_2\text{O}_3)$, whereas in the extreme O-poor (Al-rich) condition, $\mu_{\text{O}} = (1/3)\Delta H_f(\text{Al}_2\text{O}_3)$ and $\mu_{\text{Al}} = 0$. The calculated formation enthalpy of $\alpha\text{-Al}_2\text{O}_3$, $\Delta H_f(\text{Al}_2\text{O}_3) = -16.22$ eV per formula unit, is in good agreement with the experimental value of -17.04 eV.³³

The defect transition level (q/q'), is defined as the Fermi-level position below which the defect is most stable in charge state q and above which the same defect is stable in charge state q' . It can be derived from formation energies as

$$(q/q') = [E^f(D^q; \epsilon_F = 0) - E^f(D^{q'}; \epsilon_F = 0)] / (q' - q), \quad (2)$$

where $E^f(D^q; \epsilon_F = 0)$ is the defect formation energy for charge state q when ϵ_F is at the VBM. The position of the transition level in the band gap does not depend on the chemical potentials (i.e., on the growth or processing conditions).

In order to address the impact of defect levels on the electronic structure of $\text{Al}_2\text{O}_3/\text{III-V}$ interfaces, we calculate the band alignment at the $\alpha\text{-Al}_2\text{O}_3/\text{III-V}$ interface. Bulk calculations alone are insufficient to provide band offsets since they contain no absolute reference for the electrostatic potential.³⁴ To obtain band offsets, we thus performed (i) a bulk calculation to obtain the band edges relative to the average electrostatic potential, and (ii) a slab calculation to obtain the position of the average electrostatic potential in the bulk with respect to the vacuum. By combining surface and bulk calculations, we find the position of the VBM and conduction-band minimum (CBM) relative to the vacuum level. For the slab calculations, we use 12 atomic layers of GaN oriented along the nonpolar (11 $\bar{2}$ 0) direction, and a vacuum layer of 22 \AA , which are sufficiently thick to give errors of less than 0.1 eV in the calculated band offsets. For $\alpha\text{-Al}_2\text{O}_3$, a 30-atom cell oriented along the c -direction with a 13 \AA thick vacuum layer is used. The band offsets for the other III-V semiconductors were taken from previous HSE calculations that used a similar procedure.^{18,19}

III. RESULTS AND DISCUSSION

A. Native point defects

Figure 1 shows our calculated results for formation energies of native point defects in $\alpha\text{-Al}_2\text{O}_3$ as a function of the Fermi level. The Al vacancy (V_{Al}), O vacancy (V_{O}), Al interstitial (Al_i), and O interstitial (O_i) were examined. Overall, we find that V_{Al} and O_i are deep acceptors, Al_i is a deep donor, and V_{O} can act as a donor or acceptor depending on the position of the Fermi level.

The acceptor levels (0/−1), (−1/−2), and (−2/−3) of V_{Al} are at 1.4, 1.7, and 2.6 eV above the VBM, respectively. Therefore, V_{Al} is a deep acceptor, with high formation energy for Fermi-level positions near the VBM. The low formation energy for Fermi-level positions higher in the gap, under both O-rich and Al-rich conditions, indicates that V_{Al} is the dominant acceptor-type defect in intrinsic Al_2O_3 . In

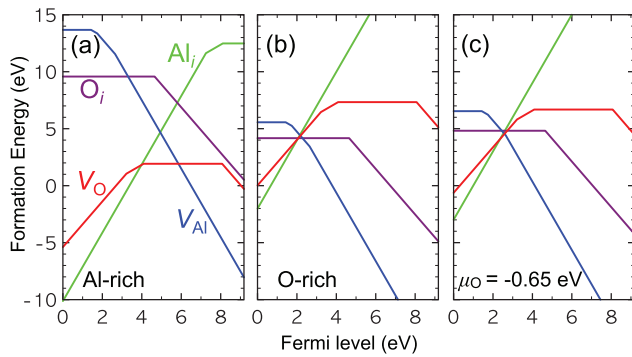


FIG. 1. Formation energies of native point defects in Al_2O_3 as a function of the Fermi level under (a) the O-rich and (b) the Al-rich limits. In panel (c) the formation energy is plotted for $\mu_{\text{O}} = -0.65$ eV, a value chosen to represent defect energetics in atomic-layer-deposited Al_2O_3 .

the -3 charge state, which is stable for all relevant Fermi-level positions, the O atoms around the vacancy relax outward by 0.15 Å.

The oxygen interstitial can assume two distinct configurations: in the neutral charge state the O_i forms a split interstitial with an O–O bond length of 1.43 Å. In the -2 charge state, O_i prefers a tetrahedral interstitial site with Al–O bond lengths of 1.86 , 1.86 , 1.90 , and 1.93 Å. The -1 state is metastable, forming a negative- U center, and the $(0/-2)$ transition level occurs at 4.7 eV above the VBM.

The oxygen vacancy has donor and acceptor levels within the gap of Al_2O_3 . It has a transition level $(+2/+1)$ at 3.2 eV and a $(+1/0)$ level at 4.1 eV above the VBM. In the $+2$ charge state the four Al atoms next to V_{O} relax outward by 0.19 – 0.29 Å, in the $+1$ charge state by 0.10 – 0.11 Å, and in the neutral charge state, the Al atoms relax inward by 0.10 Å. The $(0/-2)$ transition level is at 8.1 eV above the VBM.

The aluminum interstitial is a donor in Al_2O_3 . The transition levels of Al_i are located close to the CBM: $(+3/+1)$ at 7.3 eV and $(+1/0)$ at 8.1 eV above the VBM. The Al_i prefers to sit at the octahedral interstitial site, surrounded by O atoms with Al–O distances of 1.85 Å in the predominant $+3$ charge state, compared to 1.85 and 1.96 Å for the equilibrium Al–O distances in the bulk.

The formation energies of the donors Al_i and V_{O} are low for Fermi-level positions in the lower part of the gap. Al_i and V_{O} are therefore the dominant compensating donors in Al_2O_3 .

Al_2O_3 as a dielectric in gate stacks is most often deposited using the ALD technique. While translating ALD growth conditions into chemical-potential values is difficult, we think it reasonable to assume equilibrium with O_2 gas at 270 °C and 1 Torr, resulting in $\mu_{\text{O}} = -0.65$ eV. The values of defect formation energies in this case are shown in Fig. 1(c). Under these conditions, all four defects have similar formation energies when the Fermi level is 3 eV above the VBM. For $\epsilon_F < 3$ eV, Al_i^{+3} and V_{O}^{+2} become more stable, while for $\epsilon_F > 3$ eV, V_{Al}^{-3} is energetically most favorable.

B. Dangling bonds

The results reported above pertain to crystalline Al_2O_3 , whereas the dielectric oxides deposited with ALD generally form amorphous structures. In amorphous materials, the

long-range order is affected, making it difficult to study their electronic properties using finite-size supercells with periodic boundary conditions. The local structure, however, is generally similar to the crystalline material, and therefore, we expect the results reported in Sec. III A to still be relevant. The similarity between results for the α and κ phases, discussed below, confirms this general insensitivity to the details of the local structure. Amorphous structures do allow for the occurrence of another type of point defect, namely DBs. DBs may also occur at the interface with the semiconductor, similar to the case of Si-based MOS devices where such DBs are the dominant interfacial defects. In the case of Al_2O_3 , both Al and O DBs are in principle possible, both leading to levels in the band gap.

In order to perform calculations for DBs in Al_2O_3 without relying on the direct simulation of an amorphous structure, we followed an approach that had been previously applied to group-IV semiconductors^{35,36} as well as to κ - Al_2O_3 .^{3,18} For an Al DB, we first create an oxygen vacancy and then remove all Al atoms neighboring the vacancy except one. That is, three atoms among the Al neighbors to the V_{O} are removed. In this small void, all O DBs are passivated by fractional H atoms ($Z = 0.5$), ending up with an isolated Al DB. To construct an isolated oxygen DB, we follow the same procedure but also remove the Al atom with the isolated DB. This results in a small void containing only O DBs which are all, except one, passivated by fractional H atoms.

The transition levels of the DBs are calculated by adding an electron to, or removing an electron from a neutral DB, and using the bulk VBM as reference (taking account of the proper alignment of the electrostatic potential in the defect and the perfect-crystal supercells). We find that the isolated Al DB introduces $(+1/0)$ and $(0/-1)$ transition levels in the band gap at 4.9 and 6.4 eV above the VBM, respectively. The isolated O DB introduces a $(0/-1)$ level at 0.9 eV above the VBM, and it is not energetically stable in the $+1$ charge state.

C. Band alignment

In MOS devices, the Fermi level can vary over a region that roughly encompasses the band gap of the semiconductor material. This Fermi-level position determines the charge state of any defects and DBs in the dielectric, or at least in the vicinity of the oxide/semiconductor interface. The presence of charged defects and DBs near the interface leads to regions of charged traps and to fixed charges that can scatter carriers in the channel and shift the threshold voltage of the device. In addition, if defect transition levels are present in the energy region of the semiconductor band gap, they can act as traps and also cause leakage. The energetic position of the defect and DB levels within the gap of the dielectric thus determines how they influence the MOS device performance, but this assessment requires knowledge about the band alignment between the oxide and the semiconductor. We obtained these band alignments using the procedure discussed in Sec. II.

The position of defect levels and DBs in α - Al_2O_3 with respect to the band edges of III-V semiconductors is shown in Fig. 2. We find that the valence-band offsets between α - Al_2O_3 and III-V semiconductors are 1.7 eV for GaN,

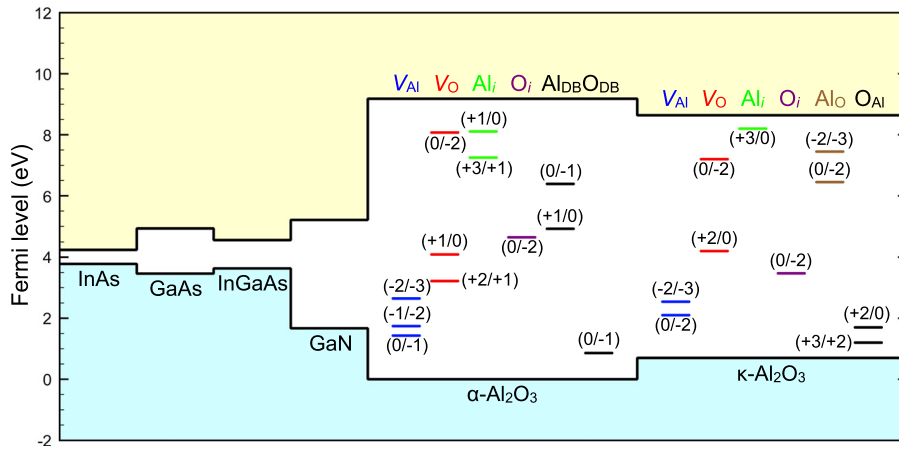


FIG. 2. Band alignment between α -Al₂O₃ and κ -Al₂O₃ and III-V compound semiconductors. The zero of energy is chosen at the VBM of α -Al₂O₃. The position of thermodynamic transition levels for native point defects and DBs in the oxides is shown with respect to the semiconductor band edges. Defect levels for κ -Al₂O₃ taken from Ref. 19 are included for comparison.

3.5 eV for GaAs, 3.8 eV for InAs, and 3.6 eV for InGaAs, with the semiconductor VBM always higher in energy than that of Al₂O₃.

For comparison, we also included in Fig. 2 the positions of defect levels in κ -Al₂O₃ taken from previous HSE calculations.^{18,19} It is noteworthy that native defects in α -Al₂O₃ exhibit similar behavior as in κ -Al₂O₃,^{18,19} despite the difference in the band gap and crystal structure of the two phases. For example, the $(-2/-3)$ transition level for V_{Al} differs by only 0.1 eV in the two phases. This similarity leads us to suggest that the positions of defect levels are not strongly dependent on the phases, i.e., on the local environment in the oxide. We therefore believe that our results for point defects in the crystalline materials are also applicable to amorphous oxides.

As shown in Fig. 2, all of the defects and DBs, except for the Al interstitial, Al_i , produce transition levels in the vicinity of the GaN band gap. Al_i induces transition levels well above the GaN CBM, acting as a fixed-charge center stable in the +3 charge state.

V_{Al} has three transition levels near the GaN VBM: the $(-1/-2)$ level at the VBM, and the $(-2/-3)$ level at 0.9 eV above the VBM; the $(0/-1)$ level is 0.3 eV below the VBM. V_{Al} thus acts as a fixed-charge center if $\epsilon_F > 0.9$ eV, which will be the case for all n -type devices.

V_O and O_i introduce charge-state transition levels in the upper part of the GaN band gap. The $(+2/+1)$ level of V_O lies 2.0 eV below the CBM, and the $(+1/0)$ level 1.1 eV below the CBM. For O_i $(0/-2)$, a single transition level is positioned at 0.5 eV below the GaN CBM. These defect levels associated with V_O and O_i lie close to the GaN CBM. In order to clarify the role of those defects, we also calculated the corresponding charge-state switching levels. During MOS device operation, the Fermi level may be modulated much more quickly than the time scale associated with defect-associated atomic relaxations due to change in the defect charge. In this case, charge-state switching levels are more relevant for determining the role of defects in the dielectrics.^{37,38} Charge-state switching levels are obtained by performing the calculation of the defect in the final charge state in the same atomic configuration as in the initial charge state. These levels are relevant for phenomena such as border traps or leakage currents through the dielectric, allowing electrons to tunnel into or out of them during device operation.

The calculated charge-state switching levels associated with V_O and O_i are shown in Fig. 3. All of these levels were obtained by fixing the atomic configuration, and then either adding or removing an electron to determine the switching level.^{37,38} We discuss the levels mainly from the perspective of their impact on n -type devices. For V_O , one set of levels is located at 2.0 and 2.8 eV above the α -Al₂O₃ VBM, which corresponds to 3.2 and 2.4 eV below the GaN CBM. A second set of levels is located at 4.4 and 5.4 eV above the α -Al₂O₃ VBM, which is 0.8 eV below and 0.2 eV above the GaN CBM. It is this second set of levels, located close to the GaN CBM, that indicates that V_O may lead to border traps and increased leakage current through the gate dielectric. In contrast, the charge-state switching levels for O_i occur far from the GaN CBM, and hence such levels will not induce border traps or leakage current in Al₂O₃/GaN MOS structures, although O_i may still act as a fixed-charge center.

Turning now to DBs, we find the $(0/-1)$ level of the oxygen DB at 0.8 eV below the VBM of GaN. Hence oxygen DBs will act as negative fixed-charge centers if present near the Al₂O₃/GaN interface. The Al DB transition levels are located near the GaN CBM; the $(+1/0)$ level lies 0.3 below the CBM and the $(0/-1)$ level lies 1.2 eV above the CBM, indicating that Al DBs can act as charge trap if present near the Al₂O₃/GaN interface.

Recent experiments⁷ on Al₂O₃ grown by ALD on n -GaN indicate the presence of charge traps at the interface

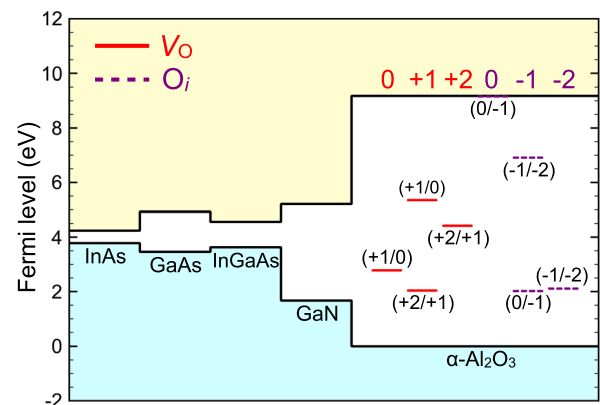


FIG. 3. Charge-state switching levels for V_O (solid) and O_i (dashed line) in α -Al₂O₃. The atomic configurations for which the levels were obtained are indicated above the corresponding levels.

that can assume neutral and positive charge states. These results can be explained by the presence of V_O and/or Al DBs. The transition levels associated with Al interstitials lie well above the GaN CBM; and V_{Al} , O_i , and O DBs may act as negative fixed charges but their levels are too far from the GaN CB to act as traps.

Positive fixed charges located near the ALD- Al_2O_3/n -GaN interface in metal/ Al_2O_3 /GaN capacitors, corresponding to interface states above the GaN CBM, have been suggested as a cause of the observed non-zero field in the oxide under flat-band conditions in GaN.³⁹ Among the native point defects, only Al_i can introduce such positive fixed charge, since it is stable in the +3 charge state when the Fermi level is near the GaN CBM.

Finally we comment on interfaces with InGaAs. Figures 2 and 3 show that among the native point defects, only V_O will have defect levels that can introduce border traps or cause leakage current in α - Al_2O_3 /InGaAs structures. For V_O , we find the (+1/0) transition level at 0.5 eV and the (+2/+1) level at 1.4 eV below the InGaAs CBM. The charge-state switching levels lie at 0.8 eV above and 0.2 eV below the InGaAs CBM and at 0.8 and 1.6 eV below the InGaAs VBM. Although O_i introduces a (0/-2) transition level near to the InGaAs CBM, the charge-state switching levels are positioned far from the InGaAs band gap. That is, those levels occur a few eV above the InGaAs CBM or below the InGaAs VBM. Other native point defects and DBs introduce defect levels located far from the semiconductor band edges, hence they will act as the fixed-charge centers but not as traps. These results for α - Al_2O_3 /InGaAs interfaces are consistent with the previous HSE calculations of κ - Al_2O_3 /InGaAs interfaces.^{3,19}

IV. SUMMARY

We have reported results of hybrid functional calculations for native point defects and dangling bonds in α - Al_2O_3 , as well as band alignments with III-V semiconductors. Based on the results, we predict that some of the defects are likely to play an important role in the performance Al_2O_3 /III-V semiconductor-based MOS devices. We find that the overall features of native defects in α - Al_2O_3 are similar to those in κ - Al_2O_3 , although the band gap and crystal structure of the two phases are different. Oxygen vacancies introduce donor levels near midgap and a (0/-2) acceptor level close to the CBM, while oxygen interstitials are deep acceptors, with a (0/-2) transition level near midgap. Al interstitials are deep donors with transition levels high in the gap, while Al vacancies are deep acceptors with transition levels near the oxide VBM; hence, these defects are unlikely to act as charge traps at Al_2O_3 /III-V interfaces, but they will play a role as fixed-charge centers. The oxygen vacancies introduce transition levels near the CBM of GaN and InGaAs, and hence can introduce border traps or cause leakage current through the gate dielectric in Al_2O_3/n -GaN and Al_2O_3/n -InGaAs MOS devices.

ACKNOWLEDGMENTS

This work was supported by the ONR DEFINE MURI (N00014-10-1-0937) and by the UCSB Solid State Lighting

and Energy Center. Computational resources were provided by the Center for Scientific Computing at the CNSI and MRL (an NSF MRSEC, DMR-1121053) (NSF CNS-0960316), and by the Extreme Science and Engineering Discovery Environment (XSEDE), supported by NSF (OCI-1053575 and DMR07-0072N).

¹*Fundamentals of III-V Semiconductor MOSFETs*, edited by S. Oktyabrsky and P. D. Ye (Springer, 2010).

²E. J. Kim, L. Wang, P. M. Asbeck, K. C. Saraswat, and P. C. McIntyre, *Appl. Phys. Lett.* **96**, 012906 (2010).

³B. Shin, J. R. Weber, R. D. Long, P. K. Hurley, C. G. V. de Walle, and P. C. McIntyre, *Appl. Phys. Lett.* **96**, 152908 (2010).

⁴G. W. Paterson, S. J. Bentley, M. C. Holland, I. G. Thayne, J. Ahn, R. D. Long, P. C. McIntyre, and A. R. Long, *J. Appl. Phys.* **111**, 104112 (2012).

⁵J. Hu and H.-S. P. Wong, *J. Appl. Phys.* **111**, 044105 (2012).

⁶Y. C. Chang, W. H. Chang, H. C. Chiu, L. T. Tung, C. H. Lee, K. H. Shiu, M. Hong, J. Kwo, J. M. Hong, and C. C. Tsai, *Appl. Phys. Lett.* **93**, 053504 (2008).

⁷N. Nepal, N. Y. Garces, D. J. Meyer, J. K. Hite, M. A. Mastro, and C. R. Eddy, Jr., *Appl. Phys. Express* **4**, 055802 (2011).

⁸K. Matsunaga, T. Tanaka, T. Yamamoto, and Y. Ikuhara, *Phys. Rev. B* **68**, 085110 (2003).

⁹J. Carrasco, J. R. B. Gomes, and F. Illas, *Phys. Rev. B* **69**, 064116 (2004).

¹⁰N. D. M. Hine, K. Frensch, W. M. C. Foulkes, and M. W. Finnis, *Phys. Rev. B* **79**, 024112 (2009).

¹¹F. Oba, A. Togo, I. Tanaka, J. Paier, and G. Kresse, *Phys. Rev. B* **77**, 245202 (2008).

¹²M. Choi, F. Oba, and I. Tanaka, *Appl. Phys. Lett.* **98**, 172901 (2011).

¹³M. Choi, F. Oba, and I. Tanaka, *Phys. Rev. B* **83**, 214107 (2011).

¹⁴A. Janotti, J. B. Varley, P. Rinke, N. Umezawa, G. Kresse, and C. G. Van de Walle, *Phys. Rev. B* **81**, 085212 (2010).

¹⁵J. L. Lyons, A. Janotti, and C. G. Van de Walle, *Phys. Rev. Lett.* **108**, 156403 (2012).

¹⁶P. Ágoston, K. Albe, R. M. Nieminen, and M. J. Puska, *Phys. Rev. Lett.* **103**, 245501 (2009).

¹⁷D. Liu, S. J. Clark, and J. Robertson, *Appl. Phys. Lett.* **96**, 032905 (2010).

¹⁸J. R. Weber, A. Janotti, and C. G. Van de Walle, *Microelectron. Eng.* **86**, 1756 (2009).

¹⁹J. R. Weber, A. Janotti, and C. G. Van de Walle, *J. Appl. Phys.* **109**, 033715 (2011).

²⁰J. Heyd, G. E. Scuseria, and M. Ernzerhof, *J. Chem. Phys.* **118**, 8207 (2003).

²¹A. V. Krulkau, O. A. Vydrov, A. F. Izmaylov, and G. E. Scuseria, *J. Chem. Phys.* **125**, 224106 (2006).

²²P. E. Blöchl, *Phys. Rev. B* **50**, 17953 (1994).

²³G. Kresse and J. Hafner, *Phys. Rev. B* **48**, 13115 (1993).

²⁴R. H. French, *J. Am. Ceram. Soc.* **73**, 477 (1990).

²⁵A. I. Kuznetsov, V. N. Abramov, V. V. Mürk, and B. P. Namozov, *Sov. Phys. Solid State* **33**, 1126 (1991).

²⁶R. E. Newnham and Y. M. de Haan, *Z. Kristallogr.* **117**, 235 (1962).

²⁷C. G. Van de Walle and J. Neugebauer, *J. Appl. Phys.* **95**, 3851 (2004).

²⁸F. Oba, M. Choi, A. Togo, and I. Tanaka, *Sci. Technol. Adv. Mater.* **12**, 034302 (2011).

²⁹C. Freysoldt, J. Neugebauer, and C. G. Van de Walle, *Phys. Rev. Lett.* **102**, 016402 (2009).

³⁰C. Freysoldt, J. Neugebauer, and C. G. Van de Walle, *Phys. Status Solidi B* **248**, 1067 (2011).

³¹K. P. Huber and G. Herzberg, *Molecular Spectra and Molecular Structure IV: Constants of Diatomic Molecules* (Van Nostrand Reinhold, New York, 1979).

³²R. Evarestov, E. Blokhin, D. Gryaznov, E. A. Kotomin, R. Merkle, and J. Maier, *Phys. Rev. B* **85**, 174303 (2012).

³³D. Ghosh and D. A. R. Kay, *J. Electrochem. Soc.* **124**, 1836 (1977).

³⁴L. Kleinman, *Phys. Rev. B* **24**, 7412 (1981).

³⁵J. R. Weber, A. Janotti, P. Rinke, and C. G. Van de Walle, *Appl. Phys. Lett.* **91**, 142101 (2007).

³⁶C. G. Van de Walle and R. A. Street, *Phys. Rev. B* **49**, 14766 (1994).

³⁷P. E. Blöchl and J. H. Stathis, *Phys. Rev. Lett.* **83**, 372 (1999).

³⁸P. E. Blöchl and J. H. Stathis, *Physica B* **273-274**, 1022 (1999).

³⁹M. Esposito, S. Krishnamoorthy, D. N. Nath, S. Bajaj, T.-H. Hung, and S. Rajan, *Appl. Phys. Lett.* **99**, 133503 (2011).